

Highlights

THz optical response of $\text{Ba}(\text{Fe}_{1-x}\text{Ni}_x)_2\text{As}_2$ films analyzed within the three-band Eliashberg s_{\pm} -wave model

Yurii A. Aleshchenko, Andrey V. Muratov, Elena S. Zhukova, Lenar S. Kadyrov, Boris P. Gorshunov, Giovanni A. Ummarino, Ilya A. Shipulin

- Using terahertz spectroscopy the temperature dependences of the superconducting condensate plasma frequency, superfluid density and London penetration depth were obtained for the underdoped, optimally doped, and overdoped $\text{Ba}(\text{Fe}_{1-x}\text{Ni}_x)_2\text{As}_2$ thin films with Ni concentrations $x = 0.035, 0.05, \text{ and } 0.08$.
- The experimental data were analyzed in the framework of the simple three-band Eliashberg s_{\pm} -wave model under the assumption that the superconducting coupling mechanism is mediated by antiferromagnetic spin fluctuations.
- The temperature dependences of the superconducting gaps were calculated.
- The choice of the model parameters was supported by the results of independent experiments.

THz optical response of $\text{Ba}(\text{Fe}_{1-x}\text{Ni}_x)_2\text{As}_2$ films analyzed within the three-band Eliashberg s_{\pm} -wave model

Yurii A. Aleshchenko^{a,*}, Andrey V. Muratov^a, Elena S. Zhukova^b, Lenar S. Kadyrov^b, Boris P. Gorshunov^b, Giovanni A. Ummarino^{c,d}, Ilya A. Shipulin^a

^a*P.N. Lebedev Physical Institute, Russian Academy of Sciences, Leninskiy Prospekt 53, Moscow, 119991, , Russia*

^b*Moscow Institute of Physics and Technology, Institutskiy per. 9, Dolgoprudny, 141700, Moscow Region, Russia*

^c*Istituto di Ingegneria e Fisica dei Materiali, Dipartimento di Scienza Applicata e Tecnologia, Politecnico di Torino, Corso Duca degli Abruzzi 24, Torino, 10129, , Italy*

^d*National Research Nuclear University MEPhI (Moscow Engineering Physics Institute), Kashirskoe shosse 31, Moscow, 115409, , Russia*

Abstract

The uncertainty of the nature of the normal state and superconducting condensate of unconventional superconductors continues to stimulate considerable speculation about the mechanism of superconductivity in these materials. Of particular interest are the type of symmetry of the order parameter and the basic electronic characteristics of the superconducting and normal states. We report the derivation of temperature dependences of the superconducting condensate plasma frequency, superfluid density, and London penetration depth by measuring terahertz spectra of conductivity and dielectric permittivity of the $\text{Ba}(\text{Fe}_{1-x}\text{Ni}_x)_2\text{As}_2$ thin films with different Ni concentrations. A comprehensive analysis of the experimental data was performed in the framework of the simple three-band Eliashberg model under the assumption that the superconducting coupling mechanism is mediated by antiferromagnetic spin fluctuations. The results of independent experiments support the choice of model parameters. Based on calculations of the

*Corresponding author

Email address: aleshchenkoya@lebedev.ru (Yurii A. Aleshchenko)

temperature dependences of superconducting gaps, we may conclude that the obtained results are compatible with the scenario, in which $\text{Ba}(\text{Fe}_{1-x}\text{Ni}_x)_2\text{As}_2$ is a multiband superconductor with s_{\pm} -wave pairing symmetry.

Keywords: Multiband superconductivity, Fe-based superconductors, Eliashberg equations, THz spectroscopy

PACS: 74.70.Xa, 74.20.Fg, 74.25.Kc, 74.20.Mn, 74.25.Gz

1. Introduction

The discovery of high-temperature superconductivity in the iron-based superconductors (IBS) has received great attention over the past 15 years [1, 2, 3, 4, 5]. Among these materials, probably the most promising and intensively studied is the 122-type family (AFe_2As_2 with $\text{A} = \text{Ba}, \text{Sr}, \text{Ca}, \text{Eu}$), for which large and high-quality single crystals can be readily grown. The 122 parent compounds are antiferromagnetic metals for which a long-range antiferromagnetic order with a spin density wave (SDW) develops with temperature decrease down to $T_N \approx 138$ K (for, e.g., BaFe_2As_2), accompanied with a structural first-order phase transition from tetragonal to orthorhombic phase. Superconductivity in the IBS can occur through chemical doping, which leads to extra holes [6], electrons [7], or chemical pressure (for isovalent substitution) [8], or by applying external pressure [9]. The Fermi surface in the Ba122 family pnictides with electron doping consists of hole barrels near the Γ point of the Brillouin zone and electron barrels near the M point [10], where several superconducting (SC) gaps could develop below critical temperature (T_c). The widely accepted pairing state of these compounds is the fully gapped s_{\pm} phase [11, 12].

There is a general consensus that spin fluctuations play an important role in the formation of Cooper pairs in pnictides. These compounds are the most recent example of systems for which BCS theory fails [13] and an Eliashberg approach is necessary to correctly describe their physics for the presence of a strong interband coupling.

Some of the most important superconductor properties, such as SC gap values, optical characteristics, temperature dependences of the London penetration depth ($\lambda_L(T)$) and superfluid density ($\rho_{SC}(T)$) can be obtained from the terahertz (THz) measurements. However, as concerned the electron-doped $\text{Ba}(\text{Fe}_{1-x}\text{Ni}_x)_2\text{As}_2$, such studies have been previously performed only by us for the optimally doped samples [14]. In addition, a large scatter of ex-

perimental order parameters (Δ) for different compositions of $\text{Ba}(\text{Fe}_{1-x}\text{Ni}_x)_2\text{As}_2$ has been observed in the literature [15, 16, 17, 18].

In this paper, for the first time we compare the SC properties of the $\text{Ba}(\text{Fe}_{1-x}\text{Ni}_x)_2\text{As}_2$ underdoped ($x = 0.035$), optimally doped ($x = 0.05$), and overdoped ($x = 0.08$) films probed by the THz spectroscopy and analyzed in the framework of the multiband Eliashberg model.

2. Experiment

The $\text{Ba}(\text{Fe}_{1-x}\text{Ni}_x)_2\text{As}_2$ films ($x = 0.035, 0.05, \text{ and } 0.08$) with the thicknesses of 100–150 nm were grown by pulsed laser deposition (PLD) method on double-polished (001) CaF_2 single-crystalline substrates using a KrF excimer laser with a 248 nm wavelength, pulse duration of 25 ns, and repetition rate of 7 Hz. The base pressure of the chamber was below 1×10^{-8} mbar and slightly increased to about 2×10^{-7} mbar during the deposition process. More details on the sample preparation can be found in [19, 20, 21, 22]. The produced films have a mirror-like surface and similar epitaxial quality with growth orientation along the c axis as the films described in [22]. The composition of the films was explored by EDX measurements. The resistivity measurements of the films were performed by the standard four-probe technique in the Van der Paw scheme. The transition temperatures evaluated at 90% of the normal state resistance are 21.1 K, 21.6 K, and 10.3 K for $x = 0.035, 0.05, \text{ and } 0.08$, respectively. In the case when the critical temperature is determined as the temperature of maximum of the derivative of resistivity with respect to temperature, the T_c values are the following: 20.27 K ($x = 0.035$), 20.36 K ($x = 0.05$), and 9.27 K ($x = 0.08$). The temperature-dependent DC resistivity of the $\text{Ba}(\text{Fe}_{1-x}\text{Ni}_x)_2\text{As}_2$ films is shown in Fig. 1(a). Note narrow (about 2 K) transition to the SC state for all films and resistivities comparable to single crystals [23], which attests the structural quality of the deposited films. In the case of the $x = 0.035$ film, we can see a semiconductor-like $\exp(-\alpha/k_B T)$ behavior (α is a constant), since at low doping this material is more similar to the insulating parent compound. The similar behavior of resistivity occurs for high-temperature SC cuprates [24]. The magnetotransport measurements of the films were performed in a physical property measurement system PPMS-9 (Quantum Design) using external magnetic fields up to 9 T along the c -axis [21]. The measured $R(T)$ curves recalculated to the temperature dependences of the resistivity in various magnetic fields are shown in Figs. 1(b)–1(d).

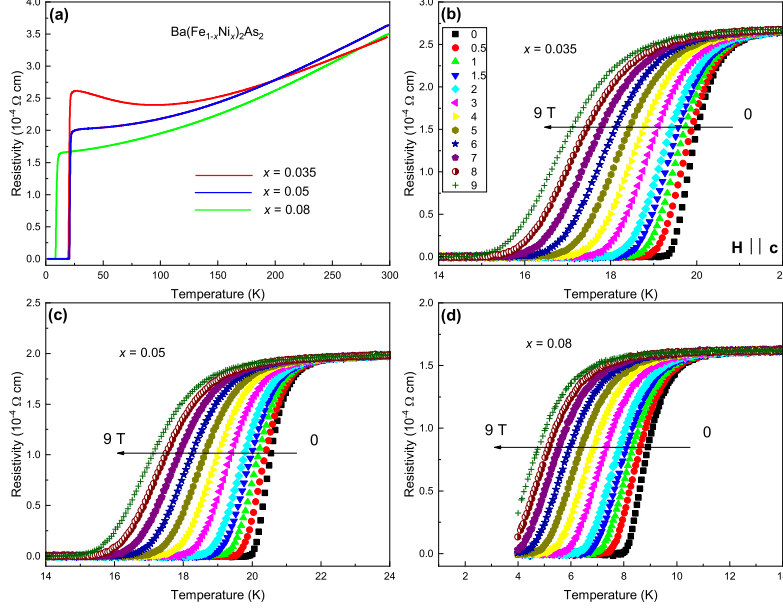


Figure 1: (Color online) Temperature dependences of the resistivity for the $\text{Ba}(\text{Fe}_{1-x}\text{Ni}_x)_2\text{As}_2$ films without magnetic field (a) and in magnetic fields 0–9 T for $x = 0.035$ (b), $x = 0.05$ (c), and $x = 0.08$ (d) (recalculated from the resistance curves [21]).

THz spectroscopic measurements were carried out in the transmission mode with the Menlo pulsed time-domain THz spectrometer within the range of $10\text{--}50\text{ cm}^{-1}$ (wavelengths $1\text{ mm} - 200\text{ }\mu\text{m}$) at different temperatures down to $T = 4\text{ K}$ with a home-made optical cryostat. Temperature-dependent THz spectra of the real and imaginary parts of the complex dielectric permittivity $\hat{\epsilon} = \epsilon_1(\omega) + i\epsilon_2(\omega)$ and the complex optical conductivity $\hat{\sigma}(\omega) = \sigma_1(\omega) + i\sigma_2(\omega)$ were determined directly without using the Kramers-Kronig relations [25], by measuring the spectra of the complex transmission coefficient $\text{Tr}(\epsilon_1, \epsilon_2)\exp[i\varphi^T(\epsilon_1, \epsilon_2)]$ or $\text{Tr}(\sigma_1, \sigma_2)\exp[i\varphi^T(\sigma_1, \sigma_2)]$ of a two-layer system (a film on a substrate), see Eq. (6) in the Appendix. Using TeraCalc software, the numerical solution of the system of two essentially non-linear equations for the amplitude $\text{Tr}(\epsilon_1, \epsilon_2)$, or $\text{Tr}(\sigma_1, \sigma_2)$, and the phase $\varphi^T(\epsilon_1, \epsilon_2)$, or $\varphi^T(\sigma_1, \sigma_2)$, at each fixed frequency and temperature provided

the spectra of the required optical parameters of the film. The dielectric properties of the CaF_2 substrate were measured beforehand.

3. THz electrodynamics of $\text{Ba}(\text{Fe}_{1-x}\text{Ni}_x)_2\text{As}_2$ films

To study the optical properties of the $\text{Ba}(\text{Fe}_{1-x}\text{Ni}_x)_2\text{As}_2$ films in detail, the response of charge carriers in the THz spectral range was analyzed, as in our previous paper [14]. The spectra of the real parts of dielectric permittivity ε_1 and conductivity σ_1 of the $\text{Ba}(\text{Fe}_{1-x}\text{Ni}_x)_2\text{As}_2$ films are shown in Figs. 2–4.

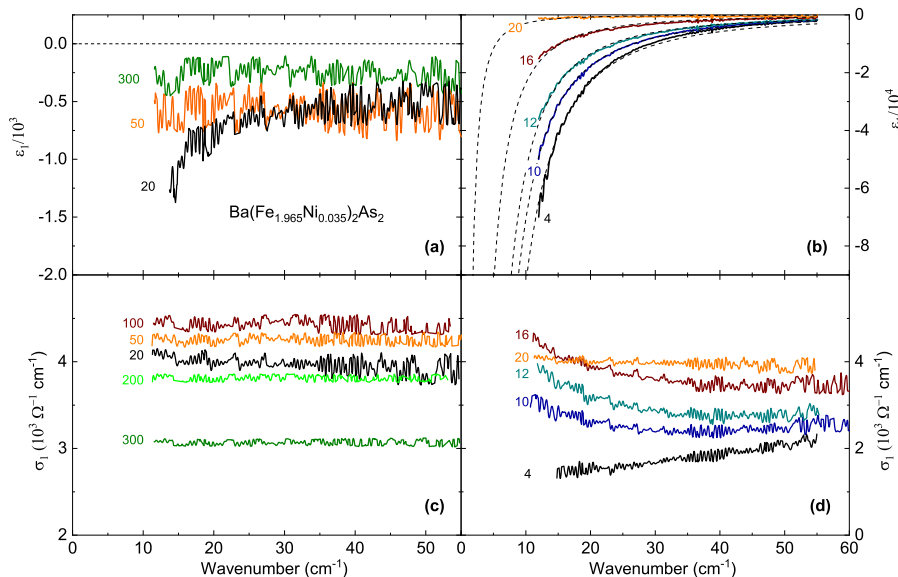


Figure 2: (Color online) Spectra of the permittivity ε_1 and the conductivity σ_1 of the $\text{Ba}(\text{Fe}_{0.965}\text{Ni}_{0.035})_2\text{As}_2$ films in the normal (a,c) and SC (b,d) states (numbers indicate temperature in Kelvins). Dashed lines in (b) show a fit of the spectra by the relation $\varepsilon_1 \propto -(\omega_{p,s}/\omega)^2$.

The dependences for the normal state are presented in Figs. 2(a,c), 3(a,c), and 4(a,c), while those for the SC state are depicted in Figs. 2(b,d), 3(b,d), and 4(b,d). In the normal state, both ε_1 and σ_1 are nearly dispersionless and increase with cooling, thereby exhibiting metallic transport typical for the low-frequency limit (frequencies far below carrier scattering rate) of the

Drude conductivity model [26]. For the films with $x = 0.05$ and $x = 0.08$ nickel contents, we observe at 20 K a slight decrease of conductivity with increasing frequency, indicating that the scattering rate approaches our operating frequency range from above [26]. In the SC state, THz conductivity of the films with Ni content $x = 0.035$ and $x = 0.05$ is strongly suppressed due to the opening of a SC gap. This suppression is accompanied by the emergence of a pronounced dispersion of permittivity shown in Figs. 2(b) and 3(b), which is a "Kramers-Kronig image" of the zero-frequency SC delta function in the conductivity spectra. This behavior is fitted by the expression $\varepsilon_1 = -(\omega_{p,s}/\omega)^2$ (dotted lines), where $\omega_{p,s}$ is a SC plasma frequency. This fit allows us to determine $\omega_{p,s}$. Note that the conductivity of the $x = 0.05$ film reaches nearly zero values around 10 cm^{-1} , while the conductivity of the $x = 0.035$ film remains rather large, indicating a larger below-gap absorption. It is easily recognized that even at the lowest temperature (4 K) for all Ni contents the gapping is not complete. We have previously demonstrated [15] that, at least for the optimally doped $\text{Ba}(\text{Fe}_{0.95}\text{Ni}_{0.05})_2\text{As}_2$, only the narrow Drude component is gapped. According to [27], the presence of a low-frequency finite conductivity well into the SC state of iron pnictides could be also due to a gap anisotropy of the electron pocket [28, 29, 30, 31]; impurity localized levels inside an isotropic SC gap [32, 33, 34, 35, 36]; or pair breaking due to interband impurity scattering in an s_{\pm} symmetric gap [37, 38]. We also observe a decrease below 100 K of the normal-state conductivity for $x = 0.035$ film, which is related to the semiconductor-like $\rho(T)$ behavior discussed above.

In the case of the film with $x = 0.08$, we can see at low temperatures a significant inductive response of the SC delta-function in the permittivity spectra (Fig. 4(b)). However, only a slight suppression of the conductivity is observed at the lowest attainable in our experiments temperature of 4 K (Fig. 4(d)), indicating that the suppression of conductivity due to the opening of a SC gap at $T = 4 \text{ K}$ is below 10 cm^{-1} .

Figures 5, 6, and 7 show the calculated temperature dependences of the SC plasma frequency ($\omega_{p,s}$) and the London penetration depth (λ_L) (right scale) of the $\text{Ba}(\text{Fe}_{1-x}\text{Ni}_x)_2\text{As}_2$ films determined as $\lambda_L = c/\omega_{p,s}$ [39] (where c is the speed of light). The temperature dependence of the superfluid density $\rho_{sc} = [\lambda_L(0)/\lambda_L(T)]^2$ is shown in the insets (a) of Figs. 5 and 6. For the $\text{Ba}(\text{Fe}_{0.92}\text{Ni}_{0.08})_2\text{As}_2$ films, we failed to obtain a reliable experimental dependence of the ρ_{sc} because of too low T_c .

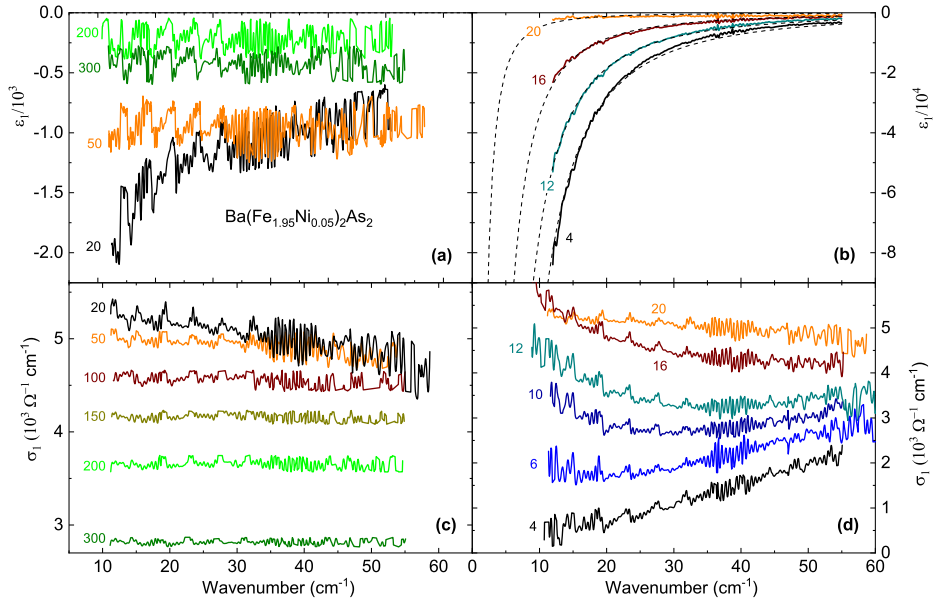


Figure 3: (Color online) Spectra of the permittivity ε_1 and the conductivity σ_1 of the $\text{Ba}(\text{Fe}_{0.95}\text{Ni}_{0.05})_2\text{As}_2$ films in the normal (a,c) and SC (b,d) states (numbers indicate temperature in Kelvins). Dashed lines in (b) show a fit of the spectra by the relation $\varepsilon_1 \propto -(\omega_{p,s}/\omega)^2$.

4. Multiband Eliashberg theory

We try to explain the experimental data in the framework of s_{\pm} multi-band Eliashberg theory [40, 41, 42, 43, 44]. Due to the fact that the electronic structure of Ba122 compounds doped with Ni or Co is extremely similar, it can be described in the framework of the three-band model [45], which assumes the presence of one hole band and two electron bands. In this case, the hole band gap (Δ_1) has opposite sign to the gaps of the two electron bands (Δ_2 and Δ_3). Despite the fact that this model is rather simple and has only two free parameters, it manages to reflect the basic physics of this class of compounds. To date, it is generally believed that in these materials the interband coupling between the hole and electron bands (s_{\pm} -wave model [46, 12]) is provided mainly by antiferromagnetic spin fluctuations (sf), while phonons can be responsible for the intraband coupling (ph) [12].

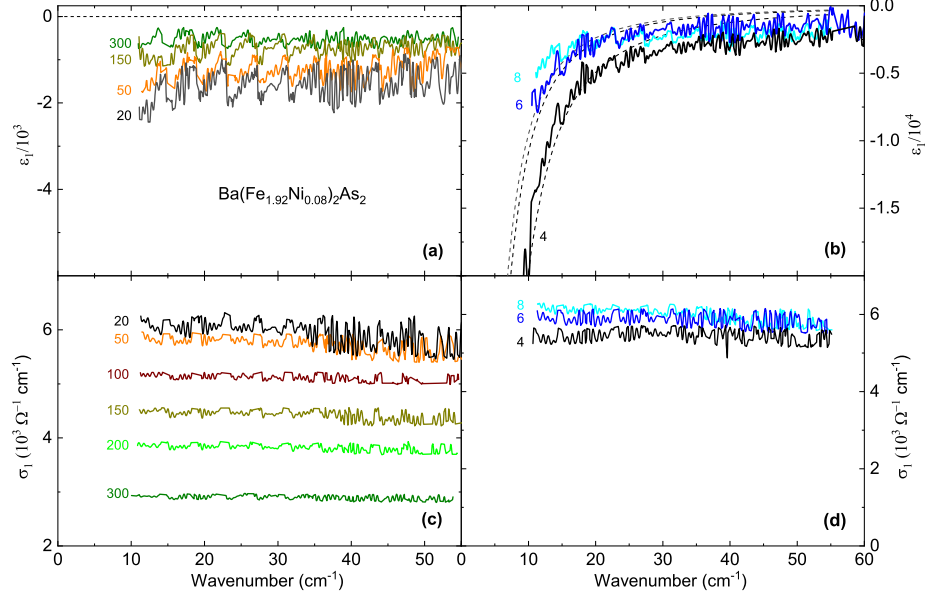


Figure 4: (Color online) Spectra of the permittivity ε_1 and the conductivity σ_1 of the $\text{Ba}(\text{Fe}_{0.92}\text{Ni}_{0.08})_2\text{As}_2$ films in the normal (a,c) and SC (b,d) states (numbers indicate temperature in Kelvins). Dashed lines in (b) show a fit of the spectra by the relation $\varepsilon_1 \propto -(\omega_{p,s}/\omega)^2$.

The calculation of basic superconducting parameters, such as the SC gaps as well as the critical temperature, can be done in the framework of the s_{\pm} -wave three-band Eliashberg equations, involving six coupled equations for the gaps $\Delta_i(i\omega_n)$ and the renormalization functions $Z_i(i\omega_n)$, where i is a band index (that ranges between 1 and 3) and ω_n are the Matsubara frequencies. The imaginary-axis equations [48, 49, 50], when the Migdal theorem works [51], read:

$$\begin{aligned} \omega_n Z_i(i\omega_n) = & \omega_n + \pi T \sum_{m,j} \Lambda_{ij}^Z(i\omega_n, i\omega_m) N_j^Z(i\omega_m) + \\ & + \sum_j [\Gamma_{ij} + \Gamma_{ij}^M] N_j^Z(i\omega_n); \end{aligned} \quad (1)$$

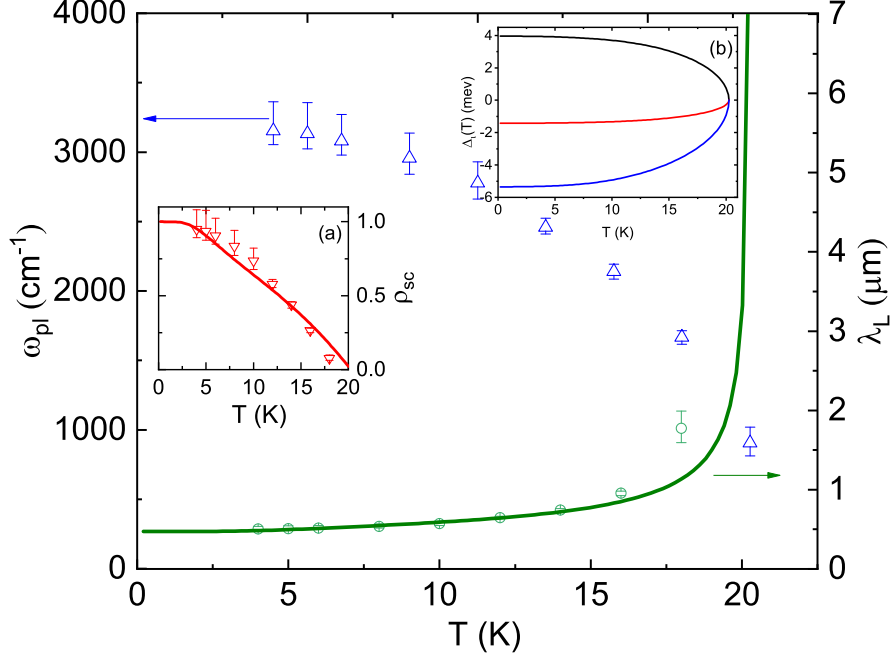


Figure 5: (Color online) London penetration depth as a function of temperature for the $\text{Ba}(\text{Fe}_{0.965}\text{Ni}_{0.035})_2\text{As}_2$ films (right scale): experimental data (open symbols) and theoretical calculations (solid green line). The temperature dependence of the plasma frequency of the SC condensate is also shown (left scale). The inset (a) shows the experimental temperature dependence of superfluid density $\rho_{sc} = [\lambda_L(0)/\lambda_L(T)]^2$ (open symbols) as well as the theoretical calculation (solid curve). The calculated SC gaps vs. temperature are presented in the inset (b). Here, the black curve represents the temperature dependence of the SC gap for the hole band, while the red and blue curves stand for the SC gaps of the two electron bands.

$$\begin{aligned}
Z_i(i\omega_n)\Delta_i(i\omega_n) &= \pi T \sum_{m,j} [\Lambda_{ij}^\Delta(i\omega_n, i\omega_m) - \mu_{ij}^*(\omega_c)] \times \\
&\times \Theta(\omega_c - |\omega_m|) N_j^\Delta(i\omega_m) + \sum_j [\Gamma_{ij} - \Gamma_{ij}^M] N_j^\Delta(i\omega_n), \quad (2)
\end{aligned}$$

where Γ_{ij} and Γ_{ij}^M are the scattering rates from non-magnetic and magnetic impurities, respectively,

$$\Lambda_{ij}^Z(i\omega_n, i\omega_m) = \Lambda_{ij}^{ph}(i\omega_n, i\omega_m) + \Lambda_{ij}^{sf}(i\omega_n, i\omega_m)$$

and

$$\Lambda_{ij}^\Delta(i\omega_n, i\omega_m) = \Lambda_{ij}^{ph}(i\omega_n, i\omega_m) - \Lambda_{ij}^{sf}(i\omega_n, i\omega_m),$$

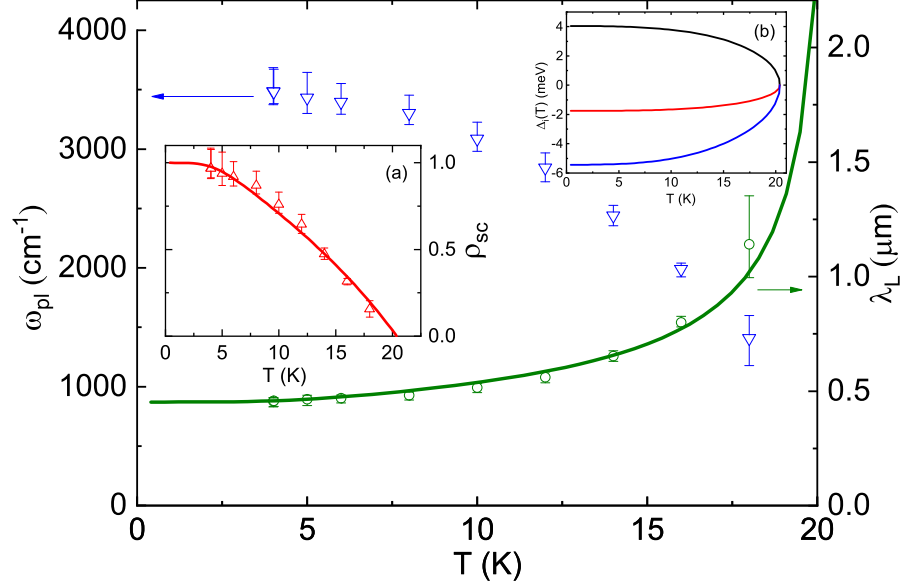


Figure 6: (Color online) London penetration depth as a function of temperature for the $\text{Ba}(\text{Fe}_{0.95}\text{Ni}_{0.05})_2\text{As}_2$ films (right scale): experimental data (open symbols) and theoretical calculations (solid green line). The temperature dependence of the plasma frequency of the SC condensate is also shown (left scale). The inset (a) shows the experimental temperature dependence of superfluid density $\rho_{sc} = [\lambda_L(0)/\lambda_L(T)]^2$ (open symbols) as well as the theoretical calculation (solid curve). The calculated SC gaps vs. temperature are presented in the inset (b). Here, the black curve represents the temperature dependence of the SC gap for the hole band, while the red and blue curves stand for the SC gaps of the two electron bands.

where

$$\Lambda_{ij}^{ph,sf}(i\omega_n, i\omega_m) = 2 \int_0^{+\infty} d\Omega \Theta(\Omega) \alpha_{ij}^2 F^{ph,sf}(\Omega) / [(\omega_n - \omega_m)^2 + \Omega^2].$$

Θ is the Heaviside function and ω_c is a cutoff energy. The quantities $\mu_{ij}^*(\omega_c)$ are the elements of the 3×3 Coulomb pseudopotential matrix. Finally, $N_j^\Delta(i\omega_m) = \Delta_j(i\omega_m) / \sqrt{\omega_m^2 + \Delta_j^2(i\omega_m)}$ and $N_j^Z(i\omega_m) = \omega_m / \sqrt{\omega_m^2 + \Delta_j^2(i\omega_m)}$. The electron-boson coupling constants are defined as

$$\lambda_{ij}^{ph,sf} = 2 \int_0^{+\infty} d\Omega \frac{\alpha_{ij}^2 F^{ph,sf}(\Omega)}{\Omega}.$$

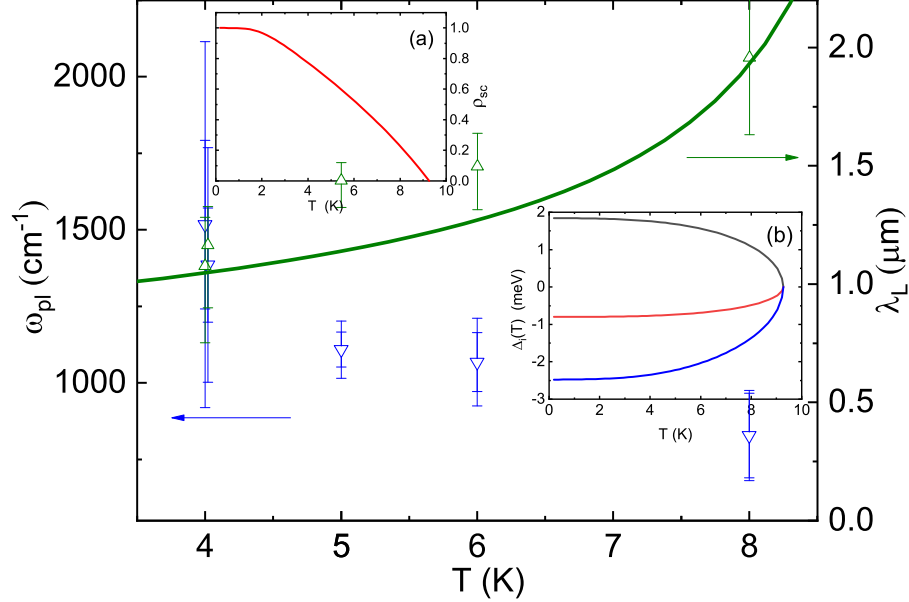


Figure 7: (Color online) London penetration depth as a function of temperature for the $\text{Ba}(\text{Fe}_{0.92}\text{Ni}_{0.08})_2\text{As}_2$ films (right scale): experimental data (open symbols) and theoretical calculations (solid green line). The temperature dependence of the plasma frequency of the SC condensate is also shown (left scale). The inset (a) shows the theoretical temperature dependence of superfluid density $\rho_{sc} = [\lambda_L(0)/\lambda_L(T)]^2$. The calculated SC gaps vs. temperature are presented in the inset (b). Here, the black curve represents the temperature dependence of the SC gap for the hole band, while the red and blue curves stand for the SC gaps of the two electron bands.

The solution of equations 1 and 2 requires a huge number of input parameters (18 functions and 27 constants), i.e.: i) nine electron-phonon spectral functions $\alpha_{ij}^2 F^{ph}(\Omega)$; ii) nine electron-antiferromagnetic spin fluctuation spectral functions, $\alpha_{ij}^2 F^{sf}(\Omega)$; iii) nine elements of the Coulomb pseudopotential matrix $\mu_{ij}^*(\omega_c)$; iv) nine nonmagnetic Γ_{ij} and nine paramagnetic Γ_{ij}^M impurity-scattering rates. However, some of these parameters can be extracted from experiments and some can be fixed by suitable approximations. In particular, we refer to experimental data taken on high quality films, thus we can rather safely assume a negligible disorder: so we can put the interband scattering from nonmagnetic and magnetic impurities Γ_{ij} and Γ_{ij}^M equal to zero, while the nonmagnetic intraband scattering have no effect on critical temperature

and gap values, so we can put here $\Gamma_{ij} = 0$. For the term Γ_{ii}^M , we apply Occam's razor to explain the experimental data with the minimum number of starting hypotheses and assume that it is null. To escape this possibility would require, for example, measurements of the superconducting density of states obtained through tunneling. The presence of magnetic impurities unambiguously changes the shape of the density of states [52].

At least as a starting point, let us make further assumptions that have been shown to be valid for iron pnictides [48, 49, 50]. Following ref. [12], we can thus assume that: i) the total electron-phonon coupling constant is small (the upper limit of the phonon coupling in the usual iron-arsenide compounds is ≈ 0.35 [53]); ii) phonons mainly provide *intraband* coupling so that $\lambda_{ij}^{ph} \approx 0$; iii) spin fluctuations mainly provide *interband coupling between hole and electron bands*, so that $\lambda_{ii}^{sf} \approx 0$. Moreover, we put in first approximation the small phonon *intraband* coupling $\lambda_{ii}^{ph} = 0.1$, so as, following Mazin I.I. [46], the Coulomb pseudopotential matrix: $\mu_{ii}^*(\omega_c) = \mu_{ij}^*(\omega_c) = 0$ [48, 49, 50, 46]. Within these approximations, the electron-boson coupling-constant matrix λ_{ij} becomes: [48, 49, 50]:

$$\lambda_{ij} = \begin{pmatrix} 0.1 & \lambda_{12}^{sf} & \lambda_{13}^{sf} \\ \lambda_{21}^{sf} = \lambda_{12}^{sf}\nu_{12} & 0.1 & 0 \\ \lambda_{31}^{sf} = \lambda_{13}^{sf}\nu_{13} & 0 & 0.1 \end{pmatrix}, \quad (3)$$

where $\nu_{ij} = N_i(0)/N_j(0)$ and $N_i(0)$ is the normal density of states at the Fermi level for the i -th band. The coupling constants λ_{ij}^{sf} are defined through the electron-antiferromagnetic spin fluctuation spectral functions (Eliashberg functions) $\alpha_{ij}^2 F_{ij}^{sf}(\Omega)$. Following refs. [48, 49, 50] we choose these functions to have a Lorentzian shape, i.e.:

$$\alpha_{ij}^2 F_{ij}^{sf}(\Omega) = C_{ij} \{L(\Omega + \Omega_{ij}, Y_{ij}) - L(\Omega - \Omega_{ij}, Y_{ij})\}, \quad (4)$$

where

$$L(\Omega \pm \Omega_{ij}, Y_{ij}) = \frac{1}{(\Omega \pm \Omega_{ij})^2 + Y_{ij}^2}$$

and C_{ij} are normalization constants, necessary to obtain the proper values of λ_{ij} , while Ω_{ij} and Y_{ij} are the peak energies and the half-widths of the Lorentzian functions, respectively [50]. In all these calculations, we set $\Omega_{ij} = \Omega_0$, thereby assuming that the characteristic energy of spin fluctuations is a single quantity for all the coupling channels and $Y_{ij} = \Omega_0/2$, based on the

x	λ_{12}	λ_{13}	$\lambda_{s,tot}$
$x = 0.035$	0.3100	1.4843	1.7967
$x = 0.05$	0.4100	1.4845	1.8914
$x = 0.08$	0.4100	1.4857	1.8926

Table 1: Electron-boson coupling constants for different electron doping levels of Ba(Fe_{1-x}Ni_x)₂As₂ films

x	T_c (K)	Δ_1 (meV)	Δ_2 (meV)	Δ_3 (meV)
0.035	20.27	4.24	-1.78	-5.90
0.05	20.36	4.27	-1.78	-5.93
0.08	9.27	1.94	-0.81	-2.70

Table 2: Critical temperatures and theoretically calculated SC low temperature gaps of Ba(Fe_{1-x}Ni_x)₂As₂ films for different electron doping levels

results of inelastic neutron scattering measurements [54] (just for simplicity we choose the phonon spectral functions $\alpha_{ij}^2 F_{ij}^{ph}(\Omega)$ with the same shape, same values of Ω_{ij} and Y_{ij}).

The peak energy of the Eliashberg functions can be directly associated with the experimental T_c by means of the empirical law $\Omega_0 = 2T_c/5$, which has been demonstrated to hold, at least approximately, for the IBS [4, 55]. With all these approximations, necessary to reduce the number of free parameters, this is the more simple model that can still grasp the essential physics of IBS. Within the framework of two-band models, experimental data can be reproduced, but electron-boson coupling constants have no direct physical interpretation [56]. We use a cut-off energy $\omega_c = 240$ meV and a maximum quasiparticle energy $\omega_{max} = 250$ meV. The factors ν_{ij} that enter the definition of λ_{ij} (eq. 3) are unknown, so we assume that they are equal to the Co-doped Ba122 [50], so $\nu_{12} = 1.12$ and $\nu_{13} = 4.5$. Now just two free parameters have to be determined λ_{12} and λ_{13} in the way to obtain the exact experimental critical temperature and the value of the small gap for $T \ll T_c$. We take for the small gap of the Ba(Fe_{1.965}Ni_{0.035})₂As₂ and Ba(Fe_{1.95}Ni_{0.05})₂As₂ films the value close to that found in our previous infrared studies of the Ba(Fe_{1.95}Ni_{0.05})₂As₂ films [15]. In the case of $x = 0.08$, we vary λ_{12} to obtain the experimental T_c . The obtained data are summarized in Tables 1 and 2. After this long discussion we arrived at a model with two free parameters. The best thing would be if they were calculated from first principles but this has not yet been done. The first conclusion, after de-

termining these two parameters, is that the material is in a moderate strong coupling regime and these values are consistent with other similar materials. We solve the imaginary-axis Eliashberg equations (eqs. 1 and 2) to calculate the low-temperature values of the gaps, which are actually obtained by analytical continuation of the imaginary solutions to the real axis by using the technique of the Padé approximants [57]. The temperature dependence of $\Delta_i(i\omega_{n=0})$ is shown in the insets (b) of Figs. 5, 6 and 7, calculated by the solution of imaginary axis Eliashberg equations as well as the electron-boson spectral functions.

5. Calculation of the penetration depth

The penetration depth, see Figs. 5, 6 and 7 (or the superfluid density, see relative insets (a)), can be computed starting from the gaps $\Delta_i(i\omega_n)$ and the renormalization functions $Z_i(i\omega_n)$ by [58, 59]

$$\lambda_L^{-2}(T) = \left(\frac{\omega_p}{c}\right)^2 \sum_{i=1}^3 w_i \pi T \sum_{n=-\infty}^{+\infty} \frac{\Delta_i^2(\omega_n) Z_i^2(\omega_n)}{[\omega_n^2 Z_i^2(\omega_n) + \Delta_i^2(\omega_n) Z_i^2(\omega_n)]^{3/2}}, \quad (5)$$

where $w_i = (\omega_{p,i}/\omega_p)^2$ are the weights of the single bands, $\omega_{p,i}$ is the plasma frequency of the i -th band, and ω_p is the total plasma frequency. Here, we can only act on the weights w_i^λ in order to adapt the calculation to the experimental $\lambda_L(T)$. The multiplicative factor involving the plasma frequencies derives from the fact that the low-temperature value of the penetration depth $\lambda_L(0)$ should be related to the plasma frequency by $\omega_p = c/\lambda_L(0)$. In all cases, we found $w_1 = 0.5$, $w_2 = 0.3$, and $w_3 = 0.2$, while $\lambda_L(T = 0) = 0.58 \mu\text{m}$, $\lambda_L(T = 0) = 0.45 \mu\text{m}$, and $\lambda_L(T = 0) = 0.92 \mu\text{m}$ for $x = 0.035$, 0.05 , and 0.08 , respectively.

6. Critical temperature versus magnetic field

The multiband Eliashberg model developed above can also be used to explain the experimental results of upper critical field measurements [49, 60, 61] as a function of temperature. For the sake of completeness, we give here the linearized gap equations in the presence of a magnetic field. In the following, v_{Fj} is the Fermi velocity of band j and B_{c2} is the upper critical

field:

$$\begin{aligned}\omega_n Z_i(i\omega_n) &= \omega_n + \pi T \sum_{m,j} [\Lambda_{ij}(i\omega_n - i\omega_m) + \delta_{n,m} \frac{\Gamma_{ij}}{\pi T}] \text{sign}(\omega_m), \\ Z_i(i\omega_n) \Delta_i(i\omega_n) &= \pi T \sum_{m,j} \{ [\Lambda_{ij}(i\omega_n - i\omega_m) - \mu_{ij}^*(\omega_c)] \times \\ &\quad \times \Theta(\omega_c - |\omega_m|) + \delta_{n,m} \frac{\Gamma_{ij}}{\pi T} \} \chi_j(i\omega_m) Z_j(i\omega_m) \Delta_j(i\omega_m),\end{aligned}$$

where

$$\begin{aligned}\chi_j(i\omega_m) &= (2/\sqrt{\beta_j}) \int_0^{+\infty} dq \exp(-q^2) \times \\ &\quad \times \tan^{-1} \left[\frac{q\sqrt{\beta_j}}{|\omega_m Z_j(i\omega_m)| + i\mu_B B_{c2} \text{sign}(\omega_m)} \right]\end{aligned}$$

with $\beta_j = \pi B_{c2} v_{Fj}^2 / (2\Phi_0)$. In these equations, the three bare Fermi velocities v_{Fj} are the input parameters. The number of adjustable parameters can be reduced [49] to one by assuming that, as in a free-electron gas, $v_{Fj} \propto N_N^j(0)$, so that $v_{F2} = \nu_{21} v_{F1}$ and $v_{F3} = \nu_{31} v_{F1}$. We found $v_{F1} = 8.9 \times 10^5$ m/s if all impurities relative to electronic bands are in the band two ($\Gamma_{11} = 912.3$ meV, $\Gamma_{22} = 20.7$ meV and $\Gamma_{33} = 0.0$ meV), while $v_{F1} = 8.5 \times 10^5$ m/s if all impurities relative to electronic bands are in the band three ($\Gamma_{11} = 912.3$ meV, $\Gamma_{22} = 0.0$ meV and $\Gamma_{33} = 20.7$ meV). We have examined two extreme situations for the $x = 0.05$ case. The real situation is probably among these two extreme cases. We fix the value of B_{c2} and then calculate T_c . Figure 8 demonstrates the results of the theoretical calculations, and it can be seen that in both cases the agreement with the experimental data is good for both $x = 0.05$ (triangles) and $x = 0.035$ (squares). The impurities related to electronic bands are all in the band 2 (red curve in Fig. 8) or in the band 3 (orange curve in Fig. 8). The values of Γ_{ij} are determined by the fit of resistivity that will be shown in the forthcoming paper. The electron-boson spectral function normalized to unity in the case of $x = 0.05$ is shown in the inset.

7. Discussion

Within the framework of the three-band Eliashberg model, it was possible to describe in some detail the experimental temperature dependences of the

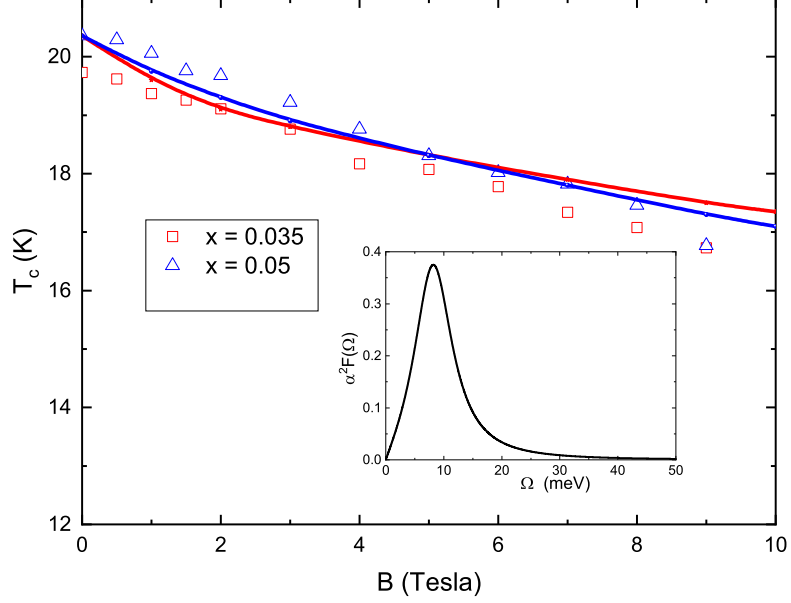


Figure 8: (Color online) The critical temperature T_c versus magnetic field B : experimental data (open symbols) and theoretical calculations (solid curves). The red and blue curves stand for the first and second cases, respectively (see the text), for $x = 0.05$ doping. The electron boson spectral function normalized to one in the case of $x = 0.05$ is shown in the inset.

superfluid density and penetration depth of the $\text{Ba}(\text{Fe}_{1-x}\text{Ni}_x)_2\text{As}_2$ films with different Ni concentrations. The calculated characteristic BCS ratios $\alpha = 2\Delta/k_B T_c = 4.9$ and 6.8 of the larger gaps for the optimal composition ($x = 0.05$) fall within the range reported in [62, 63, 64, 65, 66, 67], the characteristic ratio of the smaller gap $\alpha = 2.0$ correlates well with that found in [66, 67]. We have also determined similar characteristic ratios in our recent optical studies of the optimally doped $\text{Ba}(\text{Fe}_{0.95}\text{Ni}_{0.05})_2\text{As}_2$ films [14, 15]. Moreover, for the underdoped $\text{Ba}(\text{Fe}_{0.965}\text{Ni}_{0.035})_2\text{As}_2$ films the characteristic ratios $\alpha = 2.0, 4.7,$ and 6.5 appear to be close to the characteristics for $\text{Ba}(\text{Fe}_{0.96}\text{Ni}_{0.04})_2\text{As}_2$ single crystals [68]. It should be noted that in [18, 66, 68] three values of the order parameter were obtained and two larger ones were related to the possible anisotropic larger SC gap. Our theory predicts three SC gaps for all samples $\text{Ba}(\text{Fe}_{1-x}\text{Ni}_x)_2\text{As}_2$ ($x = 0.035, 0.05,$ and 0.08). However, in

our previous work [15], only two SC gaps were deduced from IR spectra of the $\text{Ba}(\text{Fe}_{0.95}\text{Ni}_{0.05})_2\text{As}_2$ films; it may be that one of the two gaps observed, usually the largest one, is a weighted average of the other two gaps predicted by the theory, while the smaller one is similar to that theoretically predicted.

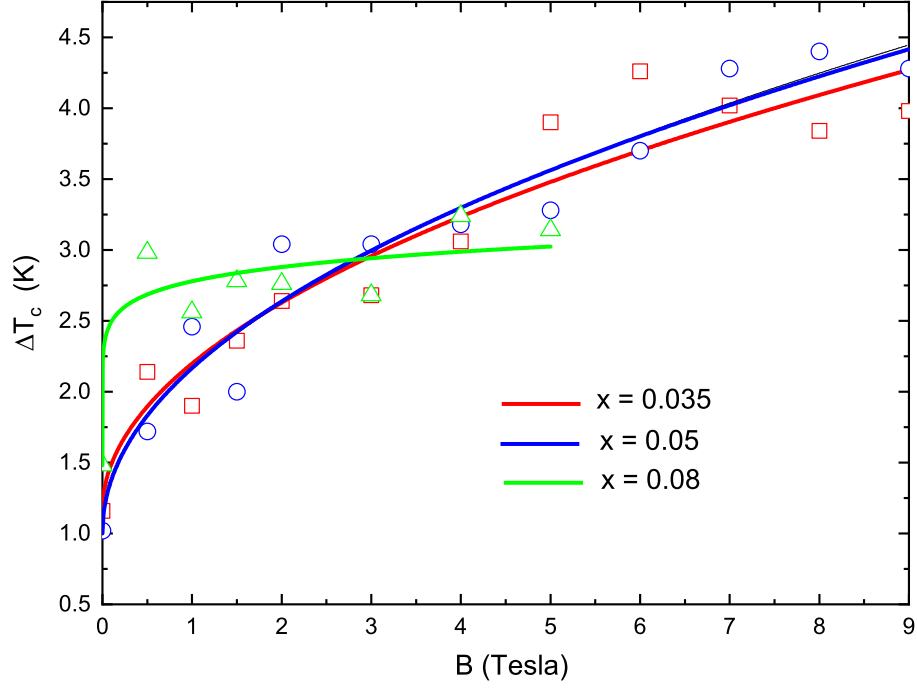


Figure 9: (Color online) The width of the resistive transition ΔT_c as a function of the applied magnetic field for Ni contents $x = 0.035$ (open red squares), $x = 0.05$ (open blue circles), and $x = 0.08$ (open green triangles). The fit with the function $\Delta T_c = a + bB^\beta$ is shown by the red solid line ($x = 0.035$, $a = 1.16000$, $b = 1.03873$, $\beta = 0.49922$), blue solid line ($x = 0.05$, $a = 1.02000$, $b = 1.16648$, $\beta = 0.48902$), and green solid line ($x = 0.08$, $a = 1.48000$, $b = 1.29929$, $\beta = 0.10741$).

Figure 9 shows the width of the resistive transition as a function of applied external magnetic field. The width of the resistive transition is defined [69] as $\Delta T_c = 2(T_c - T_{c0})$, where T_c is the critical temperature (the temperature where the derivative of the resistivity $d\rho(T)/dT$ has a maximum) and T_{c0} is the maximum temperature, where $\rho(T) = 0$. It can be shown that for the high-temperature cuprates $\Delta T_c \sim B^{2/3}$ [69], assuming that the width of the zero magnetic field transition is negligible. If this does not happen, we try

to reproduce the experimental data using a slightly more complex function of the form $\Delta T_c = a + bB^\beta$, where a , b , and β are constants [70]. For samples with concentrations of $x = 0.035$ and $x = 0.05$, we found $\beta = 0.499$ and $\beta = 0.489$, respectively, which is close to $2/3$, while for $x = 0.08$ we found $\beta = 0.107$, which diverges significantly from theoretical predictions. It is interesting to note that optimally doped $\text{Ba}(\text{Fe}_{1-x}\text{Ni}_x)_2\text{As}_2$ films have a quite similar power dependence with the high-temperature cuprates.

8. Conclusions

In this work, we have performed detailed optical conductivity measurements for the epitaxial $\text{Ba}(\text{Fe}_{1-x}\text{Ni}_x)_2\text{As}_2$ thin films ($x = 0.035, 0.05, \text{ and } 0.08$) on CaF_2 substrates in the normal and SC states using THz spectroscopy. Although a clear sign of the SC gap appears in the spectra, the conductivity does not vanish in the SC state for all Ni concentrations. A comprehensive analysis of this feature, as well as a description of the behavior of the temperature dependences of the superfluid density and the London penetration depth, was carried out in the framework of the three-band Eliashberg model. Moreover, the temperature dependences of the SC gaps were calculated on the basis of this model, which allowed us to study the features of the SC state of this compound in more details. Various independent experimental data (the temperature dependences of the upper critical magnetic field) support the choice of input parameters in the Eliashberg equations. In addition, our results are compatible with the scenario in which $\text{Ba}(\text{Fe}_{1-x}\text{Ni}_x)_2\text{As}_2$ over a wide range of Ni concentrations remains a multiband superconductor with s_\pm -wave pairing symmetry mediated mainly by antiferromagnetic spin fluctuations.

CRediT author statement

Yurii A. Aleshchenko: Conceptualization, Writing - Original Draft. **Andrey V. Muratov:** Data Curation, Formal analysis, Visualization. **Elena S. Zhukova:** Investigation. **Lenar S. Kadyrov:** Investigation. **Boris P. Gorshunov:** Writing - Original Draft, Writing - Review & Editing, Funding acquisition. **Giovanni A. Ummarino:** Methodology, Investigation, Writing - Original Draft, Visualization. **Ilya A. Shipulin:** Resources, Investigation, Writing - Review & Editing.

Declaration of competing interest

The authors declare that they have no known competing financial interests or personal relationships that could have appeared to influence the work reported in this paper.

Data availability

Data will be made available on request.

Acknowledgements

We thank Ruben Hühne for fruitful discussions and providing samples. G.A. Ummarino acknowledges partial support from the MEPhI. THz experiments were supported by the Ministry of Science and Higher Education of the Russian Federation (No. FSMG-2021-0005), THz data processing and analysis was carried out with the support of the Ministry of Science and Higher Education of the Russian Federation (Grant No. 075-15-2024-632).

Appendix

The complex transmission coefficient for the two-layer system can be evaluated using the following equation [71]:

$$T_{1234}^* = \frac{T_{12}T_{23}T_{34}e^{i(\delta_2+\delta_3)}}{1 + R_{23}R_{34}e^{2i\delta_3} + R_{12}R_{23}e^{2i\delta_2} + R_{12}R_{34}e^{2i(\delta_2+\delta_3)}}, \quad (6)$$

where T_{pq} and R_{pq} are Fresnel transmission and reflection coefficients, respectively, at the boundary between layers with indexes p and q ; $\delta_p = 2\pi d_p(n_p + ik_p)/\lambda$ for $p = 2, 3$, with d_p being the thickness of the layer p ; n_p and k_p are refraction index and extinction coefficient, respectively, of the layer p ; λ is the radiation wavelength. Namely, these coefficients can be written in exponential form, $T_{pq} = t_{pq} \exp(i\varphi_{pq}^T)$ and $R_{pq} = r_{pq} \exp(i\varphi_{pq}^R)$, and expanded through refraction index and extinction coefficient of the adjacent layers [71, 72]:

$$t_{pq}^2 = \frac{4(n_p^2 + k_p^2)}{(k_p + k_q)^2 + (n_p + n_q)^2}; \quad r_{pq}^2 = \frac{(n_p - n_q)^2 + (k_p - k_q)^2}{(k_p + k_q)^2 + (n_p + n_q)^2},$$
$$\varphi_{pq}^T = \arctg\left(\frac{k_p n_q - k_q n_p}{n_p^2 + k_p^2 + n_p n_q + k_p k_q}\right); \quad \varphi_{pq}^R = \arctg\left[\frac{2(k_p n_q - k_q n_p)}{n_p^2 + k_p^2 - n_q^2 - k_q^2}\right].$$

References

- [1] Y. Kamihara, T. Watanabe, M. Hirano, and H. Hosono, *J. Am. Chem. Soc.* **130**, 3296 (2008).
- [2] X.H. Chen, T. Wu, G. Wu, R.H. Liu, H. Chen, and D.F. Fang, *Nature (London)* **453**, 761 (2008).
- [3] G.F. Chen, Z. Li, D. Wu, G. Li, W.Z. Hu, J. Dong, P. Zheng, J.L. Luo, and N.L. Wang, *Phys. Rev. Lett.* **100**, 247002 (2008).
- [4] J. Paglione and R.L. Greene, *Nature Physics* **6**, 645 (2010).
- [5] G.R. Stewart, *Rev. Mod. Phys.* **83**, 1589 (2011).
- [6] M. Rotter, M. Tegel, and D. Johrendt, *Phys. Rev. Lett.* **101**, 107006 (2008).
- [7] A.S. Sefat, R. Jin, M.A. McGuire, B.C. Sales, D.J. Singh, and D. Mandrus, *Phys. Rev. Lett.* **101**, 117004 (2008).
- [8] S. Kasahara, T. Shibauchi, K. Hashimoto, K. Ikada, S. Tonegawa, R. Okazaki, H. Shishido, H. Ikeda, H. Takeya, K. Hirata, T. Terashima, and Y. Matsuda, *Phys. Rev. B* **81**, 184519 (2010).
- [9] P.L. Alireza, Y.T.C. Ko, J. Gillett, C.M. Petrone, J.M. Cole, G.G. Lonzarich, and S.E. Sebastian, *J. Phys.: Condens. Matter* **21**, 012208 (2008).
- [10] S. Ideta, T. Yoshida, I. Nishi, A. Fujimori, Y. Kotani, K. Ono, Y. Nakashima, S. Yamaichi, T. Sasagawa, M. Nakajima, K. Kihou, Y. Tomioka, C. H. Lee, A. Iyo, H. Eisaki, T. Ito, S. Uchida, and R. Arita, *Phys. Rev. Lett.* **110**, 107007 (2013).
- [11] A.V. Chubukov, D.V. Efremov, and I. Eremin, *Phys. Rev. B* **78**, 134512 (2008).
- [12] I.I. Mazin, D.J. Singh, M.D. Johannes, and M.H. Du, *Phys. Rev. Lett.* **101**, 057003 (2008).
- [13] O.V. Dolgov, I.I. Mazin, D. Parker, and A.A. Golubov, *Phys. Rev. B* **79**, 060502(R) (2009).

- [14] G.A. Ummarino, A.V. Muratov, L.S. Kadyrov, B.P. Gorshunov, S. Richter, A. Anna Thomas, R. Hühne, and Yu.A. Aleshchenko, *Supercond. Sci. Technol.* **33**, 075005 (2020).
- [15] Yu.A. Aleshchenko, A.V. Muratov, G.A. Ummarino, S. Richter, A. Anna Thomas, R. Hühne, *J. Phys.: Condens. Matter.* **33**, 045601 (2021).
- [16] M. Abdel-Hafiez, Y. Zhang, Z. He, J. Zhao, C. Bergmann, C. Krellner, C.-Ga. Duan, X. Lu, H. Luo, P. Dai, and X.-J. Chen, *Phys. Rev. B* **91**, 024510 (2015).
- [17] B. Zeng, B. Shen, H. Luo, G. Mu, P. Cheng, H. Yang, L. Shan, C. Ren, and H.-H. Wen, *Phys. Rev. B* **85**, 224514 (2012).
- [18] T.E. Kuzmicheva, S.A. Kuzmichev, K.S. Pervakov, and V.A. Vlasenko, *JETP Letters* **118**, 514 (2023).
- [19] S. Richter, S. Aswartham, A. Pukenas, V. Grinenko, S. Wurmehl, W. Skrotzki, B. Büchner, K. Nielsch, and R. Hühne, *IEEE Trans. Appl. Supercond.* **27**, 7300304 (2017).
- [20] S. Richter, F. Kurth, K. Iida, K. Pervakov, A. Pukenas, C. Tarantini, J. Jaroszynski, J. Hänisch, V. Grinenko, W. Skrotzki, K. Nielsch, R. Hühne, *Appl. Phys. Lett.* **110**, 022601 (2017).
- [21] I. Shipulin, S. Richter, A. Anna Thomas, M. Brandt, S. Aswartham, and R. Hühne, *Mater. Res. Express* **5**, 126001 (2018).
- [22] I. Shipulin, S. Richter, A. Anna Thomas, K. Nielsch, R. Hühne, and V. Martovitsky, *Materials* **13**, 630 (2020).
- [23] Zhaosheng Wang, Tao Xie, E. Kampert, T. Förster, Xingye Lu, Rui Zhang, Dongliang Gong, Shiliang Li, T. Herrmannsdörfer, J. Wosnitza, and Huiqian Luo, *Phys. Rev. B* **92**, 174509 (2015).
- [24] M.R. Popov, A.S. Klepikova, T.B. Charikova, E.F. Talantsev, N.G. Shelushina, and A.A. Ivanov, *Mater. Res. Express* **6**, 096005 (2019).
- [25] U.S. Pracht, E. Heintze, C. Clauss, D. Hafner, R. Bek, S. Gelhorn, D. Werner, M. Scheffler, M. Dressel, D. Sherman, B. Gorshunov, K.S. Il'in, D. Henrich, and M. Siegel, *IEEE Trans. THz Sci. Technol.* **3**, 269 (2013).

- [26] A.V. Sokolov, *Optical Properties of Metals* (Elsevier, New York, 1967).
- [27] R.P.S.M. Lobo, Y.M. Dai, U. Nagel, T. Rõõm, J.P. Carbotte, T. Timusk, A. Forget, and D. Colson, *Phys. Rev. B* **82**, 100506(R) (2010).
- [28] A.V. Chubukov, M.G. Vavilov, and A.B. Vorontsov, *Phys. Rev. B* **80**, 140515(R) (2009).
- [29] V. Mishra, G.R. Boyd, S. Graser, T. Maier, P.J. Hirschfeld, and D.J. Scalapino, *Phys. Rev. B* **79**, 094512 (2009).
- [30] J.P. Carbotte and E. Schachinger, *Phys. Rev. B* **81**, 104510 (2010).
- [31] B. Muschler, W. Prestel, R. Hackl, T.P. Devereaux, J.G. Analytis, J.H. Chu, and I.R. Fisher, *Phys. Rev. B* **80**, 180510(R) (2009).
- [32] H. Shiba, *Prog. Theor. Phys.* **40**, 435–451 (1968).
- [33] H. Shiba, *Prog. Theor. Phys.* **50**, 50–73 (1973).
- [34] A.I. Rusinov, *JETP Lett.* **9**, 85–87 (1969).
- [35] A.I. Rusinov, *Sov. Phys. JETP* **29**, 1101–1106 (1969).
- [36] E. Schachinger and J.P. Carbotte, *Phys. Rev. B* **29** 165–171 (1984).
- [37] A.B. Vorontsov, M.G. Vavilov, and A.V. Chubukov, *Phys. Rev. B* **79**, 140507(R) (2009).
- [38] E.J. Nicol and J.P. Carbotte, *Phys. Rev. B* **45**, 10519 (1992).
- [39] D.N. Basov and T. Timusk, *Rev. Mod. Phys.* **77**, 721 (2005).
- [40] G.M. Éliashberg, *Sov. Phys. JETP* **11**, 696–702 (1960).
- [41] A.V. Chubukov, D. Pines, and J. Schmalian, *A Spin Fluctuation Model for d-Wave Superconductivity*; D. Manske, I. Eremin, and K.H. Bennemann, *Electronic Theory for Superconductivity in high- T_c Cuprates and Sr_2RuO_4* , K.H. Bennemann and J.B. Ketterson Editors, Volume II. Superconductivity: Novel Superconductors, Springer-Verlag Berlin Heidelberg (2008).
- [42] J.P. Carbotte, *Rev. Mod. Phys.* **62**, 1027 (1990).

- [43] G.A. Ummarino, *Magnetochemistry* **9**, 28 (2023).
- [44] G.A. Ummarino and A. Bianconi, *Condens. Matter* **8**, 69 (2023).
- [45] G.A. Ummarino, M. Tortello, D. Daghero, and R.S. Gonnelli, *Phys. Rev. B* **80**, 172503 (2009).
- [46] P.J. Hirschfeld, M.M. Korshunov and I.I. Mazin, *Rep. Prog. Phys.* **74**, 124508 (2011); I.I. Mazin and J. Schmalian, *Physica C* **469**, 614–627 (2009).
- [47] D. Torsello, K. Cho, K.R. Joshi, S. Ghimire, G.A. Ummarino, N.M. Nusran, M.A. Tanatar, W.R. Meier, M. Xu, S.L. Bud'ko, P.C. Canfield, G. Ghigo, and R. Prozorov, *Phys. Rev. B* **100**, 094513 (2019).
- [48] G.A. Ummarino, M. Tortello, D. Daghero, R.S. Gonnelli, *Phys. Rev. B* **80**, 172503 (2009).
- [49] G.A. Ummarino, M. Tortello, D. Daghero, R.S. Gonnelli, *J. Supercond. Nov. Magn.* **24**, 247–253 (2011).
- [50] G.A. Ummarino, *Phys. Rev. B* **83**, 092508 (2011).
- [51] G.A. Ummarino and R.S. Gonnelli, *Phys. Rev. B* **56**, R14279 (1997).
- [52] A.A. Golubov and I.I. Mazin, *Phys. Rev. B* **55**, 15146 (1997).
- [53] L. Boeri, M. Calandra, I.I. Mazin, O.V. Dolgov, F. Mauri, *Phys. Rev. B* **82**, 020506(R) (2010).
- [54] D.S. Inosov, J.T. Park, P. Bourges, D.L. Sun, Y. Sidis, A. Schneidewind, K. Hradil, D. Haug, C.T. Lin, B. Keimer and V. Hinkov, *Nature Physics* **6**, 178 (2010).
- [55] D.S. Inosov, J.T. Park, A. Charnukha, Yuan Li, A.V. Boris, B. Keimer, and V. Hinkov, *Phys. Rev. B* **83**, 214520 (2011).
- [56] A. Charnukha, O.V. Dolgov, A.A. Golubov, Y. Matiks, D.L. Sun, C.T. Lin, B. Keimer, and A.V. Boris, *Phys. Rev. B* **84**, 174511 (2011).

- [57] G.A. Ummarino, Eliashbeg theory, Emergent Phenomena in Correlated Matter edited by Eva Pavarini, Erik Koch and Ulrich Schollwock, published by Forschungszentrum Julich GmbH and Institute for Advanced Simulations, 23-27 September 2013 Volume 3, Pages 13.1-13.36, ISSN 2192-8525 ISBN 978-3-89336-884-6.
- [58] G. Ghigo, G.A. Ummarino, L. Gozzelino and T. Tamegai, *Phys. Rev. B* **96**, 014501 (2017).
- [59] D. Torsello, G.A. Ummarino, J. Bekaert, L. Gozzelino, R. Gerbaldo, M.A. Tanatar, P.C. Canfield, R. Prozorov, and G. Ghigo, *Phys. Rev. Appl.* **13**, 064046 (2020).
- [60] H. Suderow, V.G. Tissen, J.P. Brison, J.L. Martínez, S. Vieira, P. Lejay, S. Lee, and S. Tajima, *Phys. Rev. B* **70**, 134518 (2004).
- [61] Y. Yerin, S.-L. Drechsler, G. Fuchs, *Journal of Low Temperature Physics* **173** (5-6), 247–263 (2013).
- [62] S. Chi, A. Schneidewind, J. Zhao, L.W. Harriger, L. Li, Y. Luo, G. Cao, Z. Xu, M. Loewenhaupt, J. Hu, and P. Dai, *Phys. Rev. Lett.* **102**, 107006 (2009).
- [63] L. Ding, J.K. Dong, S.Y. Zhou, T.Y. Guan, X. Qiu, C. Zhang, L.J. Li, X. Lin, G.H. Cao, Z.A. Xu, and S.Y. Li, *New J. Phys.* **11**, 093018 (2009).
- [64] Y. Gong, W. Lai, T. Nosach, L.J. Li, G.H. Cao, Z.A. Xu, and Y.H. Ren, *New J. Phys.* **12**, 123003 (2010).
- [65] M. Dressel, W. Dan, N. Barišić, and B. Gorshunov, *J. Phys. Chem. Solids* **72**, 514-518 (2011).
- [66] T.E. Kuzmicheva, V.A. Vlasenko, S. Gavrilkin, S.A. Kuzmichev, K.S. Pervakov, I.V. Roshchina, and V.M. Pudalov, *J. Supercond. Nov. Magn.* **29**, 3059-3064 (2016).
- [67] T.E. Kuzmicheva, S.A. Kuzmichev, A.V. Sadakov, S.Yu. Gavrilkin, A.Yu. Tsvetkov, X. Lu, H. Luo, A.N. Vasiliev, V.M. Pudalov, Xiao-Jia Chen, and Mahmoud Abdel-Hafiez, *Phys. Rev. B* **97**, 235106 (2018).

- [68] A.V. Sadakov, A.V. Muratov, S.A. Kuzmichev, O.A. Sobolevskiy, B.I. Massalimov, A.R. Prishchepa, V.M. Mikhailov, K.S. Pervakov, V.A. Vlasenko, and T.E. Kuzmicheva, *JETP Letters* **116**, 708-715 (2022).
- [69] M. Tinkham, *Phys. Rev. Lett.* **61**, 1658 (1988).
- [70] E. F. Talantsev and K. Stoltze, *Supercond. Sci. Technol.* **34**, 064001 (2021).
- [71] M. Dressel and G. Grüner, *Electrodynamics of Solids: Optical Properties of Electrons in Matter* (Cambridge University Press, New York, 2002).
- [72] V. Born and E. Wolf, *Principles of Optics* (Cambridge University Press, United Kingdom, 1999).